AIP Journal of Applied Physics

Far-field optical superlenses without metal

Charles J. Regan, Daniel Dominguez, Luis Grave de Peralta, and Ayrton A. Bernussi

Citation: J. Appl. Phys. **113**, 183105 (2013); doi: 10.1063/1.4804659
View online: http://dx.doi.org/10.1063/1.4804659
View Table of Contents: http://jap.aip.org/resource/1/JAPIAU/v113/i18
Published by the American Institute of Physics.

JOURNAL OF APPLIED PHYSICS **113**, 183105 (2013)

Far-field optical superlenses without metal

Charles J. Regan,[1,2,a)] Daniel Dominguez,[2,3] Luis Grave de Peralta,[2,3] and Ayrton A. Bernussi[1,2]

[1]*Department of Electrical and Computer Engineering, Texas Tech University, Lubbock, Texas 79409, USA*
[2]*Nano Tech Center, Texas Tech University, Lubbock, Texas 79409, USA*
[3]*Department of Physics, Texas Tech University, Lubbock, Texas 79409, USA*

(Received 18 February 2013; accepted 26 April 2013; published online 13 May 2013)

The spatial resolution in traditional optical microscopy is limited by diffraction. This prevents imaging of features with dimensions smaller than half of the wavelength (λ) of the illumination source. Superlenses have been recently proposed and demonstrated to overcome this issue. However, its implementation often involves complex sample fabrication and lossy metal layers. Alternatively, a superlens without metals can be realized using surface waves as the illumination source at the interface between two dielectrics, at the total internal reflection condition, where one of the dielectrics is doped with a fluorescent material. Non-scanning far-field images with resolution of $\sim\lambda/5$ and without the need of any post-processing or image reconstruction can be achieved with this approach. [http://dx.doi.org/10.1063/1.4804659]

I. INTRODUCTION

Traditional optical microscopy is diffraction-limited to spatial periods (p) larger than $\sim\lambda/NA$, or separation between two points, or resolution, (Δx) larger than ~ 0.5–$0.8 \times \lambda/NA$,[1,2] where λ is the free space wavelength of the illuminating light source, and NA is the numerical aperture of the microscope objective lens. Features in the sample create deviation of the transmitted light as a result of diffraction, adding parallel momentum ($k_{\|}$) to the transmitted light in accordance to the spatial frequency spectrum of the objects.[3] For objects with very small spatial period, $k_{\|}$ will be very large. The information necessary to resolve the features will be deflected past the maximum angle collectible by the microscope NA objective lens, and for nanoscale features, $k_{\|}$ will be too large to find a momentum match in the substrate and the information will be irretrievably lost in the form of evanescent waves, usually recoverable only with near-field imaging techniques.[4]

Superlenses[5–13] are a promising approach to realize an optical nanoscope which can be used as simply as a traditional optical microscope. In this work, we refer to the term superlens to describe a system which is capable of collecting the high spatial frequencies of an object which are typically lost when conventional lenses are used, therefore overcoming the well-established diffraction limit of the light predicted by Abbe's theory. Our approach dispenses the need of structural illumination, scanning or image post-processing numerical reconstruction. Real-time subwavelength images are then formed in the camera of a conventional optical microscope. This is in contrast to functional subwavelength imaging methods which require intensive numerical reconstruction, scanning, and/or sample tagging to obtain the images.[4,13–18] The images obtained by true subwavelength resolution imaging methods[5–8,11,12,19] have the same attributes as the images obtained by a traditional optical microscope.[1,2] Near-field imaging techniques with true subwavelength resolution imaging have been previously reported.[5–7] In the far-field regime, hyperlenses[8] and plasmon-coupled leakage radiation (PCLR) microcopy, also known as surface plasmon polariton (SPP) tomography,[11,12] have been used to obtain true subwavelength resolution images. The principle underlying the PCLR technique is the enhancement of the fluorescence intensity that is transmitted through a thin layer of metal via coupling with evanescent waves when compared to the intensity of the transmitted fluorescence that passes directly through the sample without exciting evanescent waves,[20] and the subsequent collection of the transmitted evanescent-coupled fluorescence by the oil immersion objective lens of a microscope.[11,12,21,22] Super-resolution is achieved because the momentum of the surface plasmons offsets the parallel momentum gained by diffraction. In the specific case of PCLR, SPP waves are generated by illuminating the top surface of the metal/glass samples which were coated with a thin fluorescent dye-doped layer. A fraction of the emitted fluorescent light couples to SPPs which propagates through the metal-dielectric interface and then leaks to the substrate.[11,12,23,24] The physical principle underlying this technique relies on the fact that the wavevector of the SPPs (k_{spp}) is subtracted from the $k_{\|}$ which is added to the light diffracted by the object, allowing information from smaller features to be transmitted into the substrate through leakage within the collection cone angle of the microscope objective lens.[11] It is important to note here that while a SPP wave propagating in a non-patterned metal-dielectric interface can be viewed as having a single wavevector, the dispersion of any propagating wave in both periodic or non-periodic structures (which can be described as the sum of periodic spatial frequencies) is modified by the presence of surface features (i.e., a non-uniform interface). As stated by Bloch theory, any wave propagating through a periodic medium must be periodic in the momentum space. This is well known from the photonic crystal theory where the dispersion of light, and thus the allowed wavevectors, is

[a)]Author to whom correspondence should be addressed. Electronic mail: cj.regan@ttu.edu.

different in a periodic medium when compared to a uniform medium of the same material. For instance, light propagating in a single mode Si waveguide (uniform) has only one momentum value in the direction of propagation. However, in a Si photonic crystal, the dispersion of light can be drastically altered where multiple, or even zero, wavevectors are allowed. The same principle applies to plasmonic crystals. For instance, the Fourier plane (FP) images of a periodic patterned surface correspond to a set of multiple rings rather than a single one observed for a uniform surface. These multiple rings are related to the Fourier transform of the features patterned in the surface of the sample.[11] This concept can be extended to non-periodic surface features. In this case, the allowed momentum will be determined by the features of the non-uniform medium in which it is propagating.

While the angular range of light coupling into (and out of) SPP plane waves is relatively narrow when propagating in a periodic medium,[11] this angular range is repeated at the angles corresponding to the original SPP wavenumber plus and minus the Fourier spectrum values of the in-plane scattering features that modify its propagation. This is critical for sensing applications since excitation of SPPs is a resonant phenomenon and may occur within very narrow angular ranges. However, because the excited SPP wave propagation is modified by the periodic scattering features in the sample surface,[11] SPP waves leak to substrate, and therefore to the far-field, at many angles where they can be collected by the high NA objective lens, contributing to the real image formation of objects.

SPP-based superlenses, however, suffer from undesired ohmic-related losses and complex sample fabrication since metal layers or alternating layer stacks are required for their realization. Recently, a far-field technique without metal layers has been demonstrated with true subwavelength-resolution based on the use of small glass beads to frustrate evanescent waves excited at the sample surface.[19] However, the far-field images obtained with this approach exhibit strong aberration and require precise positioning of the micro-beads over the nano features under observation. Therefore, simple alternative approaches to achieve optical far-field subwavelength resolution are of critical importance.

In this work, we demonstrate a simple far-field optical technique with true subwavelength-resolution which does not require metal layers. The proposed superlens relies on the combination of evanescent waves generated by excitation of dye-doped dielectric-only coated samples and the collection of leakage radiation coupled to the excited evanescent waves. However, this superlens approach is in fact a generalization, going from the specific case of using SPPs as illumination to using any surface waves existing at a general interface, in this case all-dielectric. In reality, surface waves guided by the interface of two dissimilar dielectric materials are another specific case, which along with the SPP approach in Ref. 11, suggest that the general case of any kind of surface wave used for illumination must produce similar results. Our approach is based on the selective fluorescent excitation of surface waves existing at the interface between two dielectrics. First, we demonstrate the existence of surface waves guided by the interface of two dissimilar dielectric materials, and show that they can be selectively excited fluorescently, so that the fluorophores couple preferentially into these surface waves rather than emitting in all directions. Then, we give a conceptual and experimental demonstration of how to use these surface waves guided by the interface of two dissimilar dielectric materials for super-resolution imaging using FP images. We compare the surface emission (SE) images of periodic structures to those obtained at the same wavelength using conventional optical microscopy to unambiguously show that the resolving power is indeed beyond the diffraction limit of classical optical microscopy. Then, we derive an analytical expression for the expected resolution of the superlens without a metal and compare it with that of traditional microscopy. Excellent agreement between experiment and the model was obtained. Finally, we use this expression to further enhance the resolving power of the proposed superlens.

II. EXPERIMENTS AND RESULTS

A. Fluorescent excitation of surface waves

In general, superlenses make use of excitation of surface waves to enhance their resolving power. For this reason, metals have been the typically medium of choice, as SPPs are well known to exist at the metal-dielectric interface. To produce an all-dielectric superlens, it is necessary to exploit some alternative form of surface waves at a dielectric-dielectric interface. Previously, several types of surface waves existing at dielectric-dielectric interfaces have been explored, including Zekkeck,[25–27] Tamm,[28] Dyakonov,[29,30] and Dyakonov-Tamm[31] waves. It is well-known from the Goos-Hänchen effect (GHE) that totally internally reflected light impinging from the high refractive index (n) medium generates surface waves at a dielectric-dielectric interface which propagate of the order of few wavelengths.[32–34] The magnitude of the GH shift, and thus the length of the propagation of the evanescent wave,[34–36] can be determined for both perpendicularly and parallel polarized lights as described in Refs. 33 and 34, and solved for angles of incidence larger than the critical angle as

$$L_{GH}^{p} = \frac{\lambda n_{sub}}{\pi} \frac{\sin\theta}{\sqrt{\sin^2\theta - \left(\frac{\mathrm{n_{sup}}}{\mathrm{n_{sub}}}\right)^2}}, \tag{1}$$

$$L_{GH}^{s} = L_{GH}^{p} \frac{\left(\frac{\mathrm{n_{sup}}}{\mathrm{n_{sub}}}\right)^2}{\sin^2\theta\left(1 + \left(\frac{\mathrm{n_{sup}}}{\mathrm{n_{sub}}}\right)^2\right) - \left(\frac{\mathrm{n_{sup}}}{\mathrm{n_{sub}}}\right)^2}. \tag{2}$$

In Eqs. (1) and (2), λ is the free space wavelength of light, θ is the angle formed with the normal of the light incident from the high index substrate, and $\mathrm{n_{sub}}$ and $\mathrm{n_{sup}}$ are the refractive indexes of the substrate and superstrate, respectively (in our case, $\mathrm{n_{sup}} \sim 1$ will be neither the refractive index of the air nor the PolyMethylMethAcrylate (PMMA) which both lie above the glass substrate but an average of both with

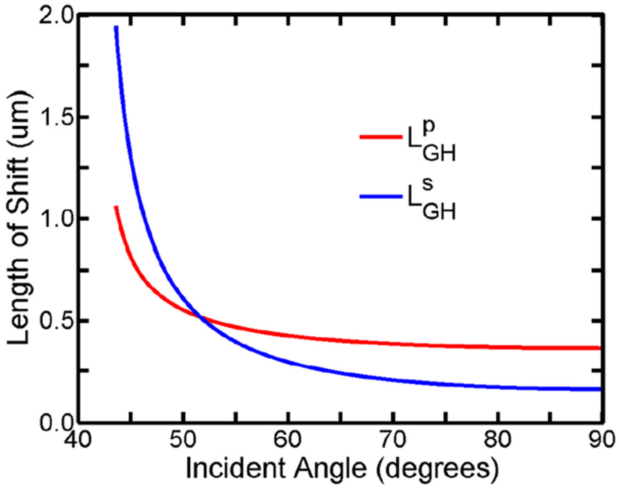

FIG. 1. Simulated magnitude of Goos-Hanchen shift at $\lambda = 568$ nm wavelength as a function of the angle of incidence for light travelling from glass to air for both *s*- and *p*-polarizations.

respect to how much of the evanescent wave field lies within each, considering that the evanescent field will extend through the PMMA and also exist within the air). The magnitude of the shift (surface wave propagation) is plotted in Figure 1 for $\lambda \sim 568$ nm and for both polarizations, versus the angle of incidence, for all angles larger than the critical angle. It is important to note that the maximum value of the length of the propagation of the evanescent wave is of the order of several wavelengths. While classically these surface waves are excited by impinging light from the high-n dielectric past the critical angle, efficient excitation by fluorescence of evanescent waves was originally demonstrated by coating the top face of a hemispherical prism with fluorescent material[37,38] Following this method, we experimentally confirmed that surface waves can be excited fluorescently by fluorophores lying within the near-field of the interface on the low-n side of the interface. By momentum match, these surface waves will "leak" to the substrate at all angles larger than the critical angle. This is a phenomenon we term the reciprocal Goos-Hänchen effect (rGHE). In analogy to the PCLR approach, the rGHE method for exciting leaky waves at a dielectric-dielectric interface is to the classical GHE as the PCLR fluorescence technique is to the Kretschmann configuration for exciting SPPs at a metal-dielectric interface; in other words, reciprocal processes of each other. We thus denote here this technique as rGHE-superlens.

Figure 2(a) illustrates the schematic of the cross-section of a uniform layer used in our experiments. This sample is solely used to demonstrate that these dielectric-dielectric surface waves can indeed be excited fluorescently, and will then leak at all angles larger than the critical angle. The samples consisted of ~110 nm thick layer of PMMA doped with Rhodamine-6G (R6G) spun on the top of a ~150 μm thick glass coverslip, all lying on top of a high *NA* immersion oil microscope objective lens ($NA = 1.49$). Using the same experimental arrangement described in Refs. 11 and 12, and shown in Fig. 2(b), the fluorophores were excited from the top using a continuous-wave laser emitting at 532 nm wavelength. The fluorescent emission, centered at ~568 nm wavelength, excites surface waves guided by the interface of two dissimilar dielectric materials. These waves travel a distance of the order of several wavelengths at the glass/PMMA interface[32–34] before leaking to the substrate in a direction determined by the momentum of the surface waves. The leaked light is collected by the immersion oil microscope objective lens, band-pass filtered at 568 nm wavelength, and then imaged on both the SE and the FP cameras of the microscope. Fig. 2(c) shows the FP image corresponding to a uniform sample (see Fig. 2(a)). The bright, thick ring observed in the FP image (Fig. 2(c)) corresponds to a map of the momentum, or equivalently the effective refractive index n_{eff} of the surface waves guided by the interface of two dissimilar dielectric materials propagating at the glass/PMMA-R6G interface. In this case, we define n_{eff} as $k_{//}/k_0$, where $k_{//}$ is the wavenumber of the surface wave parallel to the interface, and k_0 is the free-space wavenumber. The ring radius is proportional to n_{eff} while the width of the ring indicates that modes with different n_{eff} are excited. This is critical evidence that we are indeed exciting surface waves guided by the interface of two dissimilar dielectric materials fluorescently,

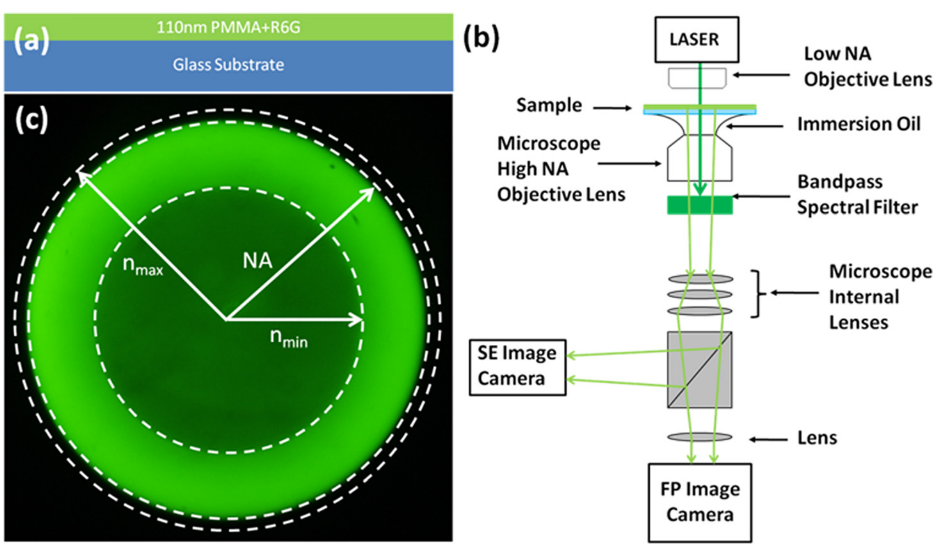

FIG. 2. (a) Schematic illustration of a uniform sample comprising of a thin R6G-PMMA layer spun on the top of glass substrate, (b) experimental setup used to excite all-dielectric surface waves and image the resulting leaked light, and (c) measured FP image of a R6G-PMMA(110 nm thick)/glass.

and that the light is in fact leaking with angles larger than the critical angle. If the surface waves were not present, or were not being selectively coupled to, one would no longer expect a ring (light emitted in certain defined angles), but rather a uniform disk where the fluorescent light would be emitting in all possible angles, with angular intensity modified by the transmission function of light travelling from air into glass. However, as shown in Figure 3 from Fresnel's equations, this modification of the intensity due to the transmission function for both polarizations of incident light has a maximum in the center, which is the opposite of our experimental data, suggesting that surface waves are modifying the transmission function.

The image shown in Fig. 2(c) is different from the thin bright ring typically observed in the FP images of SPPs from a uniform coated sample using PCLR microscopy.[11,39] The thin ring corresponds to the resonant angle of the SPP which leaked to the substrate. In contrast, surface waves guided by the interface of two dissimilar dielectric materials exist for wavevectors matching *all* angles larger than the critical angle. Therefore, n_{eff} of the surface modes will vary from $n_{min} = n_{superstrate}$ to $n_{max} = n_{substrate}$, where $n_{superstrate}$ and $n_{substrate}$ are the refractive indexes of the media on top and at the bottom of the dielectric-dielectric interface, respectively. This can be directly determined from Fig. 1(c) using standard FP calibration procedures.[39] In the case of dielectric-only superlenses with $n_{min} \sim 1$, the surface mode "sees" mostly an air superstrate since the PMMA-R6G layer is very thin, and $n_{max} \sim 1.525$ corresponds to the glass substrate used in our experiments. However, the angle corresponding to n_{max} cannot be imaged since it is larger than the maximum collecting angle of the objective lens ($NA = 1.49$) used in our microscope. Therefore, the thick ring is cut off at the NA of the microscope objective lens. This observation is central to a later discussion, because it indicates that a metal layer is not necessary to fluorescently excite surface waves, and that the emission of fluorophores can be modified by the near-field placement of a dielectric-dielectric interface. It is also critical to note here that these surface waves are *not* being excited through total internal reflection from light emitted from the high-n dielectric side of the interface, but instead the fluorescence is coupled directly into the available surface modes from the low-n side of the interface, similarly to the case of plasmon-coupled emission.[22]

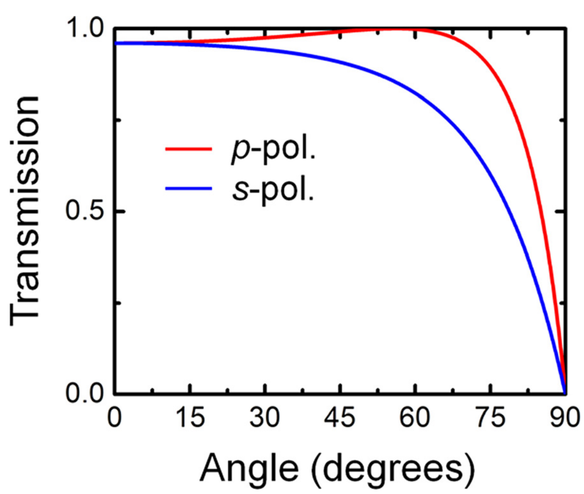

FIG. 3. Transmission of light incident from air to glass at different incidence angles for both polarizations at 568 nm free space wavelength.

B. Mechanism of superresolution and Fourier imaging

In order to understand how these fluorescently excited surface waves guided by the interface of two dissimilar dielectric materials can be exploited to obtain super-resolution images it is instructive to compare the anticipated Fourier images when the surface waves are used as the illumination source with that from a traditional optical transmission illumination. Figure 4 shows schematic illustrations of the anticipated Fourier images of a dielectric-doped uniform surface and a periodic dielectric-doped patterned surface (square lattice) under different illumination conditions. Similar to Fig. 2, the FP image corresponding to the surface waves in a uniform doped layer (Fig. 4(a)) is represented by a thick ring defined between minimum wavenumber of the surface waves (k_{min}) that leaks at the critical angle, and the maximum collectible angle of the microscope objective lens numerical aperture (which has an effective parallel wavenumber k_{NA} and is defined by the dashed line) used in the experiments. In the camera, the image displayed will be any light falling within this dashed ring. This is an indication that all leaked light has momentum parallel to the surface, whereas for conventional transmission (Fig. 4(b)) the light is concentrated near the center, indicating that the light has little or no parallel momentum. When a periodic patterned (with square lattice symmetry) surface of a sample is illuminated by surface waves (Fig. 4(c)) and by traditional transmission illumination (Fig. 4(d)), the FP images comprise of extra rings and extra spots, respectively. In both cases, the illumination wavelength is kept constant. The center of these rings will be located at the position of the spots in the Fourier space, and the spacing between spots will be proportional to the Fourier components of the object being imaged ($G = 2\pi/p$) (in this case, the spacing will be inversely proportional to the period of the periodic object). The key to achieve super-resolution is that at object sizes where the spots formed from transmission imaging lie outside the maximum angle that the microscope NA can collect, it is possible that the rings will still exist within this angle (Fig. 4(e)). These results can be seen as a direct consequence of both diffraction and Bloch theories.

In order to achieve super-resolution images in all-dielectric structures, it is, therefore, necessary to demonstrate the situation depicted in Figure 4, or in other words to show that for fluorescent surface wave illumination the FP image consists of multiple rings, and for traditional transmission illumination, the FP image consists of multiple dots. This can be accomplished by modifying the structure shown in Fig. 2(a) by a periodic Cr object patterned on the top of the glass substrate and then covered it with R6G doped PMMA. We fabricated periodic structures consisting of cylindrical Cr pillars 35 nm tall with varying periodicity p, and diameters $d = p/2$ arranged in a square lattice symmetry. Fig. 5 shows measured FP images of a sample with $p = 500$ nm. In

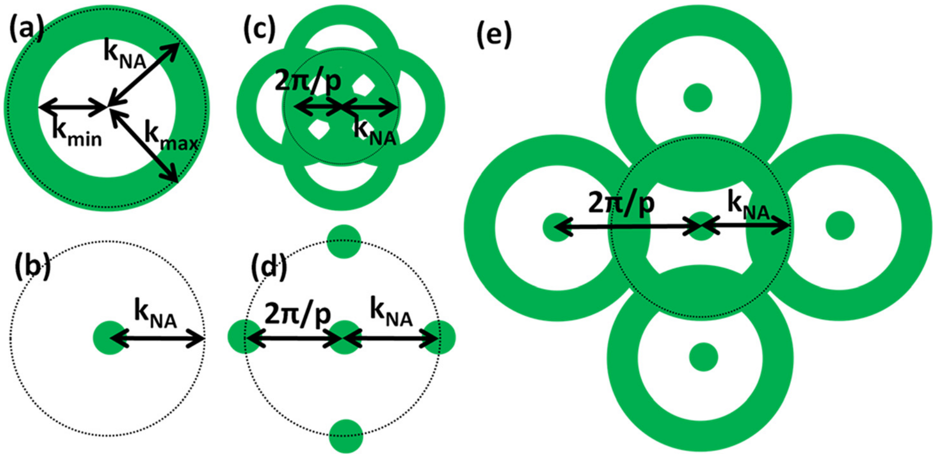

FIG. 4. Schematic illustrations of FP images expected for (a) surface wave illumination of a uniform surface, (b) traditional illumination of a uniform surface, (c) surface wave illumination of a square lattice periodic surface, (d) traditional illumination of a square lattice periodic surface, (e) the case for super-resolution imaging using all-dielectric surface waves. In all images, the maximum collectible wavenumber k_{NA} is denoted by a dashed ring.

Fig. 5(a), we confirm the existence of the extra rings as predicted by the Bloch theory when the object under interrogation is a periodic structure. The inset of Fig. 5(a) shows the extra rings with enhanced clarity, and they can be compared to Fig. 4(b). The measured FP image using traditional microscopy illumination is shown in Fig. 5(b). In this case, the top R6G PPMA layer was removed and white light illumination was used instead in combination with a bandpass filter centered at 568 nm wavelength. It is evident from Fig. 5(b) the presence of the central and the extra spots predicted by diffraction theory, in this case for a sample with $p = 380$ nm. Consequently, the information about the periodic structure is directly related to the presence of the extra rings and spots in the FP images when the sample is illuminated by surface waves or conventional transmission, respectively. This confirms the predictions illustrated in Fig. 4. Now, to demonstrate the super-resolution capability of the lens, we need to find an experimental condition (i.e., proper periodicity p) that matches the condition illustrated in Fig. 4(e).

C. Unambiguous demonstration of super-resolution surface images

To verify the super-resolution results of the superlens, we have experimentally explored the resolution limits in the surface image of the sample, using both fluorescently excited surface wave illumination as well as traditional transmission illumination. In both cases, the illumination and collection schemes were performed as described above; however, the SE camera of the microscope was used in order to obtain the images produced in the real space. We experimented with samples of different periods under both illumination schemes. Figs. 6(a) and 6(b) show SE images for two samples with $p = 240$ nm (Fig. 6(a)) and $p = 220$ nm (Fig. 6(b)), respectively, when illuminated with surface waves. It is evident for the sample with $p = 220$ nm (Fig. 6(b)) that the surface features cannot be resolved. Figs. 6(c) and 6(d) show SE images for two other fabricated samples with $p = 360$ nm (Fig. 6(c)) and $p = 320$ nm (Fig. 6(d)), respectively, under conventional transmission illumination conditions. Visibly, for periods $p < 360$ nm, the surface features cannot be resolved under traditional transmission illumination. This is a clear and unambiguous demonstration that fluorescently excited surface waves guided by the interface of two dissimilar dielectric materials can be used to produce sub-diffraction-limited images in the real plane, showing that the actual resolution of the proposed superlens occurs for spatial periods approximately 120 nm smaller than that using conventional microscopy.

D. Theoretical analysis of the expected resolution

In order to understand the results shown in Fig. 6, we first discuss the anticipated resolution for the proposed dielectric-only superlens, and compare it with that expected for an ordinary optical microscope. In conventional optical microscopy, light transmitted through a periodic lattice sample (comprising holes or pillars) produces a diffraction pattern in the FP

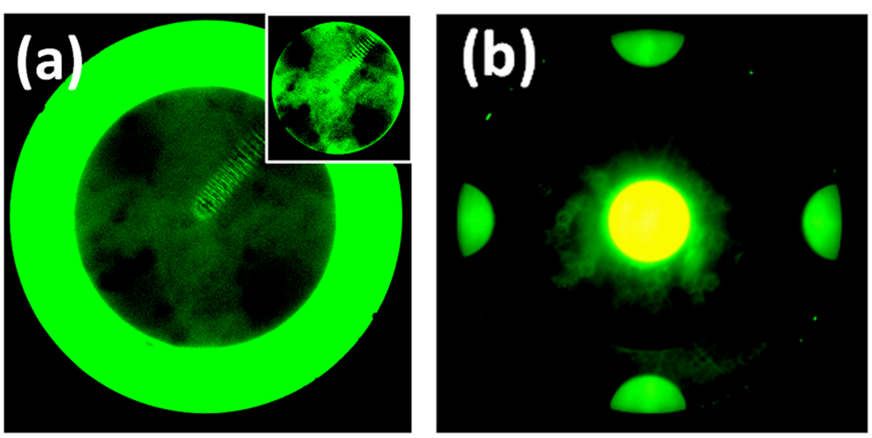

FIG. 5. FP images of periodic patterned samples with periodicity much larger than the resolving limit of each system. (a) FP image for surface wave illumination for a sample with $p = 500$ nm, and (b) FP image for traditional illumination of a sample with $p = 380$ nm.

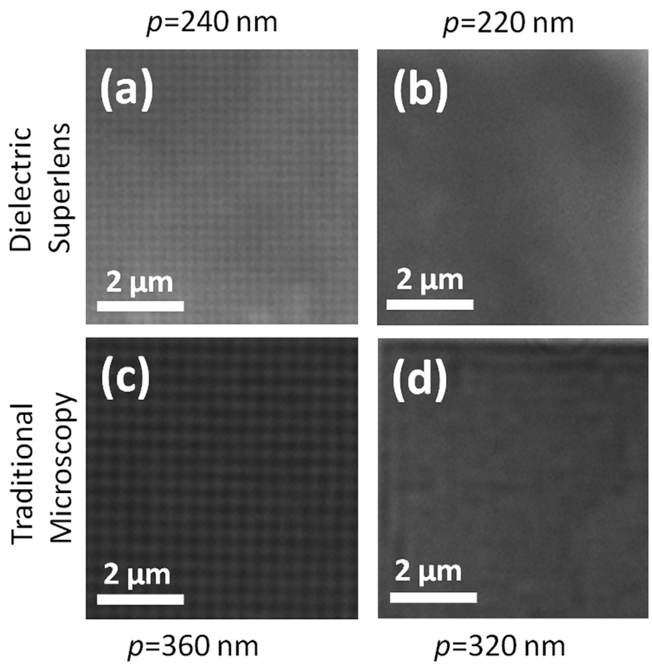

FIG. 6. SE images of periodic patterned samples obtained under different illumination conditions: surface wave illumination: (a) $p = 240$ nm and (b) $p = 220$ nm; traditional illumination: (c) $p = 360$ nm and (d) $p = 320$ nm.

where the first order diffraction spots are located at $k_{spot} \sim 2\pi/p$. This implies that the surface periodicity cannot be resolved below λ/NA, which equals $p > 380$ nm in our case, and agrees well with the experimental results shown in Figs. 6(c) and 6(d). The minimum period observable is related with the Rayleigh resolution criteria giving the minimum resolvable separation between two points, Δx, by the relation $\Delta x = p_{min}/2$.[1,11] This corresponds to the well-known value of the resolution in traditional optical microscopy of $\Delta x \sim \lambda/2\,\mathrm{NA} \sim 200$ nm. However, in our rGHE-superlens approach (as well as the PCLR-superlens), we observed in the FP image of a periodic lattice extra rings centered at the reciprocal lattice points of the crystal with a radius corresponding to $2\pi n_{eff}/\lambda$.[23,24] This is in accordance with the Bloch theory where for a wave propagating in a periodic medium the equifrequency curves in the k-space are also periodic. This has been previously demonstrated for the case of plasmonic crystals investigated by PCLR microscopy.[23,24] The optical resolution characteristics of the rGHE-superlens proposed here corresponds well to that obtained for the PCLR technique.[11,12] In the case of the PCLR superlens, the minimum period (or maximum spatial frequency) and the corresponding maximum resolution Δx are defined as[11,12]

$$p > \frac{\lambda}{NA + n_{eff}^{SPP}} \quad \text{and} \quad \Delta x > \frac{\lambda}{2(NA + n_{eff}^{SPP})}. \tag{3}$$

In Eq. (3), n_{eff}^{SPP} is the effective refractive index of the propagating SPP. This is the case where the *extra rings*, formed from scattering in the lattice, are just visible in the microscope FP[11] (whereas in traditional microscopy the limit $p > \lambda/NA$ exists where the *diffraction spots* are just visible in the microscope Fourier plane, as verified by our experiments in Figs. 5 and 6). For the case of the thick ring, as exists in rGHE, these equations must be slightly modified. No longer must the ring just be visible inside the NA, but the outside edge of the extra rings must now exist within the inside edge of the central ring (otherwise the central and extra rings overlap and the lack of contrast will blur the surface image). The minimum resolvable period and the image resolution of the rGHE superlens can then be described as

$$p > \frac{\lambda}{n_{\max} + n_{\min}} \quad \text{and} \quad \Delta x > \frac{\lambda}{2(n_{\max} + n_{\min})}. \tag{4}$$

In Eq. (4), n_{min} in Eq. (2) replaces n_{eff}^{SPP} in Eq. (3), and it is defined as the effective index corresponding to the minimum radius of the central ring, and n_{max} replaces NA, and it is defined as the maximum radius of the central ring, which corresponds to $n_{glass} = 1.525$ in our experiments. This case will exist until n_{min} exceeds the NA of the microscope setup, at which point it will be replaced by NA in the Eq. (4). However, n_{max} has no such theoretical limit. Using Eq. (4) we can calculate the new expected resolution as $p > 230$ nm, which also agrees well with the results shown in Figs. 6(a) and 6(b).

It is important to stress that the reason why subwavelength resolution images can be observed using both PCLR and rGHE superlens techniques is that in traditional transmission microscopy, the first-order spots formed by diffraction (which carries the sample periodicity information) are located at $k_{spot} \sim 2\pi/p$ in the FP image of the sample, outside the maximum collectible $k_{NA} \sim 2\pi NA/\lambda$ for features with small periods p. In contrast, the first-order diffraction rings in the FP of periodic features are located at $k_{ring} \sim (2\pi/p - 2\pi n_{eff}/\lambda)$ on both the PCLR and the proposed rGHE-superlens techniques. This k_{ring} value can, therefore, be smaller than k_{spot} for the same period p, allowing the light to exist within k_{NA} (i.e., for values of p smaller than the traditional diffraction optical limit but within the resolvable limit of the rGHE- and PCLR-superlenses, $k_{ring} < k_{NA} < k_{spot}$).

E. Further imaging resolution improvements of the rGHE superlens

According to Eq. (4) the resolution of the rGHE-superlens can be further improved by increasing n_{min}. This can be simply realized, for instance, by covering the PMMA + R6G layer with water. We fabricated two additional samples with periods $p = 220$ nm and $p = 200$ nm and covered them with drops of water. The SE of the samples with periods $p = 220$ nm and $p = 200$ nm are shown, respectively, in Figs. 7(a) and 7(b). After determining $n_{min} \sim 1.33$ from the refractive index of the new cover (water), we estimated from Eq. (4) that the new resolution limit should occur at $p \sim 200$ nm. Due to limited contrast, the results do not exactly match the calculation, but we do increase the resolution of the system and resolve Cr features with $p = 220$ nm (Fig. 7(a)), whereas for $p = 200$ nm the surface is not resolved (Fig. 7(b)). This corresponds to $\Delta x_{min} = 110$ nm, a remarkable resolution of $\lambda/5$ for such a simple setup. The rGHE-superlens resolution can be further improved using a higher refractive index material instead of water on the top surface of the sample. Index-matching fluids with refractive

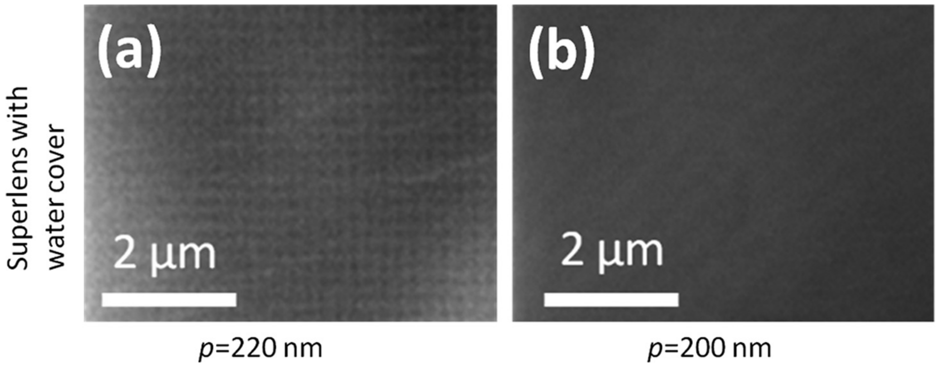

FIG. 7. SE images of periodic patterned samples covered with a drop of water: (a) $p = 220$ nm and (b) $p = 200$ nm.

index close to the glass substrate are commercially available (for instance $n \sim 1.52$ at 568 nm wavelength). In this case, we anticipate $\Delta x_{min} = \lambda/(2(1.52 + 1.49)) \sim 94.4$ nm or $\Delta x_{min} \sim \lambda/6$, which is approximately half the size of the predicted resolvable feature for traditional microscopy. Even further resolution improvements can be achieved with the rGHE-superlens by selecting a substrate with a higher refractive index than the glass ($n_{max} > n_{glass}$). Moreover, by engineering the dispersion of the surface modes to increase n_{eff}, it would be possible to enhance the resolution even more.

III. CONCLUSIONS

In summary, we have demonstrated a simple, non-scanning, far-field optical superlens without any metal layer. Real-time images that do not require any computational reconstruction or sample tagging were obtained with the proposed technique. We demonstrate that the rGHE superlens can resolve features with $\lambda/5$ resolution in the visible spectrum, and should inherently be able to be extended to other wavelength regimes. We anticipate that engineering the dielectric interface[40,41] and using high refractive index substrates the resolution of rGHE superlenses can even be further increased. This work represents a generalization of the metallic superlens[5–7,11,12] where the object under observation is not illuminated by SPPs but by surface waves guided by the interface of two dissimilar dielectric materials. We foresee the development of new types of superlenses based on the excitation of a variety of evanescent waves; for instance, recent advances in surface exciton polaritons[42,43] should result in novel far-field optical superlenses without metal.

ACKNOWLEDGMENTS

This work was partially supported by the NSF CAREER Award (ECCS-0954490).

[1]S. Durant, Z. Liu, J. M. Steele, and X. Zhang, "Theory of the transmission properties of an optical far-field superlens for imaging beyond the diffraction limit," J. Opt. Soc. Am. B **23**, 2383–2392 (2006).
[2]E. Hecht, *Optics*, 3rd ed. (Addison Wesley, MA, 1998).
[3]J. W. Goodman, *Introduction to Fourier Optics* (McGraw-Hill, New York, 1968).
[4]E. Betzig, M. Isaacson, and A. Lewis, "Collection mode near field scanning optical microscopy," Appl. Phys. Lett. **51**, 2088–2090 (1987).
[5]J. B. Pendry, "Negative refraction makes a perfect lens," Phys. Rev. Lett. **85**, 3966–3969 (2000).
[6]D. O. S. Melville, R. J. Blaikie, and C. R. Wolf, "Submicron imaging with a planar silver lens," Appl. Phys. Lett. **84**, 4403–4405 (2004).
[7]G. Tremblay and Y. Sheng, "Designing the metallic superlens close to the cutoff of the long range mode," Opt. Express **18**, 740–745 (2010).
[8]L. Zhaowei, H. Lee, Y. Xiong, C. Sun, and X. Zhang, "Far-field optical hyperlens magnifying sub-diffraction-limited objects," Science **315**, 1686 (2007).
[9]X. Zhang and Z. Liu, "Superlenses to overcome the diffraction limit," Nature Mater. **7**, 435–440 (2008).
[10]F. M. Huang, T. S. Kao, V. A. Fedotov, Y. Chen, and I. Zheludev, "Nanohole array as a lens," Nano Lett. **8**, 2469–2472 (2008).
[11]C. J. Regan, R. Rodriguez, S. Gourshetty, L. Grave de Peralta, and A. A. Bernussi, "Imaging nanoscale features with plasmon-coupled leakage radiation far-field superlenses," Opt. Express **20**, 20827 (2012).
[12]L. Grave de Peralta, C. J. Regan, and A. A. Bernussi, "SPP tomography: A simple wide-field nanoscope," Scanning **00**, 1–7 (2012).
[13]L. Zhaowei, S. Durant, H. Lee, Y. Pikus, Y. Xiong, C. Sun, and X. Zhang, "Experimental studies of far-field superlens for sub-diffractional optical imaging," Opt. Express **15**, 6947–6954 (2007).
[14]P. T. So, H. S. Kwon, and C. Y. Dong, "Resolution enhancement in standing-wave total internal reflection microscopy: A point-spread-function engineering approach," J. Opt. Soc. Am. A **18**, 2833–2845 (2001).
[15]M. G. L. Gustafsson, "Nonlinear structured-illumination microscopy wide-field fluorescence imaging with theoretical unlimited resolution," Proc. Natl. Acad. Sci. U.S.A. **102**, 13081–13086 (2005).
[16]S. W. Hell and M. Krough, "Ground-state depletion fluorescence microscopy, a concept for breaking the diffraction resolution limit," Appl. Phys. B: Lasers Opt. **60**, 495–497 (1995).
[17]X. Zhuang, "Nano-imaging with STORM," Nature Photon. **3**, 365–367 (2009).
[18]G. Shtengel, J. A. Galbraith, C. G. Galbraith, J. Lippincott-Schwartz, J. M. Gillette, S. Manley, R. Sougrat, C. M. Waterman, P. Kanchanawong, M. W. Davidson, R. D. Fetter, and H. F. Hess, "Interferometric fluorescent super-resolution microscopy resolves 3D cellular structure," Proc. Natl. Acad. Sci. U.S.A. **106**, 3125–3130 (2009).
[19]Z. Wang, W. Guo, L. Li, B. Luk'yanchuk, A. Khan, Z. Liu, Z. Chen, and M. Hong, "Optical virtual imaging at 50 nm lateral resolution with a white-light nanoscope," Nat. Commun. **2**, 218 (2011).
[20]Z. Liu, N. Fang, T. Yen, and X. Zhang, "Rapid growth of evanescent wave by silver superlens," Appl. Phys. Lett. **83**, 5184–5186 (2003).
[21]I. Gryczinski, K. Malicka, K. Nowaczyk, Z. Gryczynski, and J. Lacowicz, "Effects of sample thickness on the optical properties of surface plasmon-coupled emission," J. Phys. Chem. B **108**, 12073–12083 (2004).
[22]I. Gryczynski, J. Malicka, Z. Gryczynski, and J. R. Lacowicz, "Surface plasmon-coupled emission with gold films," J. Phys. Chem. B **108**, 12568–12574 (2004).
[23]C. J. Regan, O. Thiabgoh, L. Grave de Peralta, and A. A. Bernussi, "Probing photonic Bloch wavefunctions with plasmon-coupled leakage radiation," Opt. Express **20**, 8658 (2012).
[24]C. J. Regan, L. Grave de Peralta, and A. A. Bernussi, "Equifrequency curve dispersion in dielectric-loaded plasmonic crystals," J. Appl. Phys. **111**, 073105 (2012).
[25]A. Sihvola, J. Qi, and I. V. Lindell, "Bridging the gap between plasmonics and Zenneck waves," IEEE Antennas Propag. Mag. **52**, 124–136 (2010).
[26]V. N. Datsko and A. A. Kopylov, "On surface electromagnetic waves," Phys. Usp. **51**, 101–102 (2008).
[27]A. V. Kukushkin, "On the existence and physical meaning of the Zenneck wave," Phys. Usp. **52**, 755–756 (2009)
[28]H. Maab, M. Faryad, and A. Lakhtakia, "Prism-coupled excitation of multiple Tamm waves," J. Mod. Opt. **60**, 355–358 (2013).

[29]D. Artigas and L. Torner, "Dyakonov surface waves in photonic metamaterials," Phys. Rev. Lett. **94**, 013901 (2005).
[30]O. Takayama, L. C. Crasovan, S. K. Johansen, D. Mihalache, D. Artigas, and L. Torner, "Dyakonov surface waves: A review," Electromagnetics **28**, 126–145 (2008).
[31]J. Gao, A. Lakhtakia, and M. Lei, "Dyakanov-Tamm waves guided by the interface between two structurally chiral materials that differ only in handedness," Phys. Rev. A **81**, 013801 (2010).
[32]X. Yin and L. Hesselink, "Goos-Hänchen shift surface plasmon resonance sensor," Appl. Phys. Lett. **89**, 261108 (2006).
[33]K. Artmann, "Berechnung der Seitenversetzung des totalreflektierten Strahles," Ann. Phys. **437**, 87–102 (1948).
[34]R. H. Renard, "Total reflection: A new evaluation of the Goss-Hanchen Shift," J. Opt. Soc. Am. **54**, 1190–1197 (1964).
[35]J. S. Guasto, P. Huang, and K. S. Breuer, "Evanescent wave microscopy," *Encyclopedia of Micro- and Nano-fluidics*, edited by D. Li (Springer, 2008).
[36]A. Kodre and J. Strnad, "Model of the Goos-Haenchen effect," J. Opt. Soc. Am. **64**, 1722–1723 (1974).
[37]P. Selenyi, "Sur l'existence et l'observation des ondes lumineuses sphériques inhomogénes," Compt. Rend. **157**, 1408–1410 (1913).
[38]B. W. Smith, Y. Fan, J. Zhou, N. Lafferty, and A. Estroff, "Evanescent wave imaging in optical lithography," Proc. SPIE **6154**, 61540A (2006).
[39]S. P. Frisbie, C. F. Chesnutt, M. E. Holtz, A. Krishnan, L. Grave de Peralta, and A. A. Bernussi, "Image formation in wide-field microscopes based on leakage of surface plasmon-coupled fluorescence," IEEE Photonics Journal **1**, 153–162 (2009).
[40]F. Pillon, H. Guilles, S. Girard, and M. Laroche, "Goos-Hänchen and Imbert-Fedorov shifts for leaky guided modes," J. Opt. Soc. Am. B **22**, 1290–1299 (2005).
[41]I. V. Soboleva, V. V. Moskalenko, and A. A. Fedyanin, "Giant Goos-Hänchen and Fano resonance in photonic crystal surfaces," Phys. Rev. Lett. **108**, 123901 (2012).
[42]F. Yang, J. R. Sambles, and G. W. Bradberry, "Long-range coupled surface exciton polaritons," Phys. Rev. Lett. **64**, 559–562 (1990).
[43]V. Giannini, Y. Zhang, M. Forcales, and J. Gómez-Rivas, "Long-range surface polaritons in ultra-thin films of silicon," Opt. Express **16**, 19674–19685 (2008).